

---

## MICROCRYSTALLINE, NANOCRYSTALLINE, POROUS, AND COMPOSITE SEMICONDUCTORS

---

# Carrier Transport in Layered Semiconductor (*p*-GaSe)— Ferroelectric (KNO<sub>3</sub>) Composite Nanostructures

A. P. Bakhtinov<sup>^</sup>, V. N. Vodopyanov, Z. D. Kovalyuk, V. V. Netyaga, and D. Yu. Konoplyanko

Frantsevich Institute of Materials Science Problems, Chernivtsi Branch, National Academy of Sciences of Ukraine,  
ul. Vil'de 5, Chernivtsi, 58001 Ukraine

<sup>^</sup>e-mail: chimsp@ukrpost.ua

Submitted August 5, 2010; accepted for publication August 25, 2010

**Abstract**—The current–voltage characteristics and frequency dependences of the impedance of composite nanostructures fabricated on the basis of layered anisotropic semiconductor *p*-GaSe and ferroelectric KNO<sub>3</sub> are studied. Multilayer nanostructures were obtained by introducing nanoscale pyramidal ferroelectric inclusions into a layered GaSe matrix. Hysteresis phenomena in current–voltage characteristics and abrupt changes in the conductance and capacitance in frequency dependences of the impedance are detected. These phenomena are associated with the collective effect of electric polarization switching in nanoscale 3D ferroelectric inclusions in the layered matrix, features of its local deformation, and polytype phase transitions in this matrix. X-ray, atomic-force microscopy, and impedance studies in a low ( $B < 400$  mT) magnetic field show that the electrical characteristics of nanostructures are associated with the Maxwell–Wagner effect in nanostructures, the formation of quantum wells in GaSe during deformation of crystals in the region of nanoscale inclusion localization, and carrier tunneling in the structures.

**DOI:** 10.1134/S1063782611030067

### 1. INTRODUCTION

Nanostructures based on ferroelectric materials are of interest in relation to their use in information technologies in high-density memory systems (FeRAMs) in which the phenomenon of polarization switching by an external electric field [1] is used and in sensors, capacitors, and electrical energy storage devices [2, 3]. The sizes and shapes of ferroelectric (FE) nanoparticles, the depolarization field, surface effects, and stresses resulting from the deformation interaction between nanoparticles and matrix have a significant effect on phase states of nanoparticles and their physical properties [4]. Layered semiconductors feature anisotropic properties and molecular bonds between layers. The interlayer space (the Van der Waals gap) can be filled with foreign atoms, ions, and molecules the number of which can be comparable to or exceed the number of matrix material molecules. If a method for introducing a foreign material (from a vapor phase, electrolyte, liquid, or melt) to the crystal region where molecular forces act makes it possible to perform this process without chemical and deformation interactions between an introduced material and the matrix, such a method (intercalation) allows the formation of a multilayer nanostructure. In this structure, a two-dimensional (2D) matrix layers of the layered crystal will be arranged between intercalate layers of nanoscale thickness. The electrical properties of such intercalated crystals (e.g., graphite–bromine [5]) are well described by the model according to which they are considered to be a set of independent 2D objects

arranged along the crystallographic *C* symmetry axis. During chemical and deformation interactions that can take place between the material introduced into the matrix and the layered crystal matrix, nanoscale cavities filled with the foreign material and separated from each other are formed on Van der Waals (VdW) surfaces of layers. They encompass several crystal layers and propagate into the crystal to a depth of about several nanometers from the VdW surface [6–8]. Such a composite nanostructure can be considered as a bulk layered crystal (natural superlattice [9]) in which three-dimensional (3D) nanostructures (NSs) are incorporated. In the last few years, FE properties of NaNO<sub>2</sub> nanoparticles [10] and mixed NaNO<sub>2</sub>–KNO<sub>3</sub> FE were actively studied under constrained geometry conditions in MCM-41 nanoporous silica molecular sieves [11]; dielectric properties of these composite structures were also studied [11, 12]. Composite nanostructures consisting of nanoscale layers of semiconductor materials and FE inclusions almost have not yet been studied. In [13–15], the conductivity, permittivity, and spectral distribution of photoconductivity of InSe and GaSe layered crystals intercalated with sodium and potassium nitrite were studied. The authors of [13–15] failed to explain temperature dependences of the conductivity, permittivity, and photoconductivity spectra of these crystals within the model of a multilayer structure consisting of alternating semiconductor crystal layers (“host”) and layers with FE properties (“guest” material).

As an external electric field is applied to a composite nanostructure containing FE inclusions, electric field polarization occurs in the latter. In this case, the sizes of these inclusions change due to the inverse piezoelectric effect, which can result in LC matrix deformation. The deformation interaction between inclusions and the matrix depends on the elastic constants of these materials, features of deformation processes in the anisotropic layered crystal and in ferroelectric, and on the voltage applied to the structure. This interaction can also change due to the magneto-plastic effect in FE inclusions when the structure is under a weak external dc magnetic field [16]. Deformation of FE inclusions affects their properties [4] and changes the FE nanostructure morphology on which electric polarization switching processes depend [17]. Deformations affect the band structure of semiconductors; in the quantum-confinement structures, they control the carrier energy spectrum. They have a significant effect on the luminescence, electrical, and photoelectric properties of semiconductor layered crystals [18, 19] and nanostructures based on them [7]. It is of interest to study carrier accumulation and transport in composite nanostructures based on layered crystals and ferroelectric in the presence of the deformation interaction between the layered semiconductor matrix and nanoscale FE inclusions. In this paper, we present the results of the study of electrical properties of composite nanostructures based on a “soft” (in the sense of mechanical properties) semiconductor layered crystal GaSe and a “rigid” FE crystal  $\text{KNO}_3$  [11] at various applied voltages under a weak dc magnetic field.

## 2. EXPERIMENTAL

The structures were fabricated using undoped GaSe crystals ( $\epsilon$ -polytype) grown by the Bridgman method. The resistivity of these crystals at  $T = 300$  K was  $\sim 10^3\text{--}10^4 \Omega \text{ cm}$ ; the hole concentration was  $p \approx 10^{14} \text{ cm}^{-3}$ . Potassium nitrate compound was introduced into the interlayer space of these crystals from the melt of this compound at  $T = 335 \pm 0.5^\circ\text{C}$  [20]. X-ray diffraction analysis was performed before and after fabrication of structures using a DRON-2 X-ray diffractometer with  $\text{CuK}\alpha$  radiation ( $\lambda = 1.5418 \text{ \AA}$ ). As ohmic contacts to the structures under study, In–Ga contacts were used in electrical measurements. The area of the samples under study in the GaSe (0001) basal plane did not exceed  $0.2 \times 0.3 \text{ cm}^2$ ; the thickness was  $\sim 0.1 \text{ cm}$ . The dark current–voltage ( $I\text{--}V$ ) characteristics and impedance spectra of composite nanostructures were studied using a Solartron FRA 1255 frequency analyzer in the frequency range of  $10^{-1}\text{--}4 \times 10^6 \text{ Hz}$  at temperatures of  $220\text{--}420$  K. The voltage variation rate in the measurements of quasi-stationary  $I\text{--}V$  characteristics was  $\sim 5 \text{ mV s}^{-1}$ . The transverse ac impedance was studied at an ac signal amplitude of  $\sim 10 \text{ mV}$  and various dc bias voltages

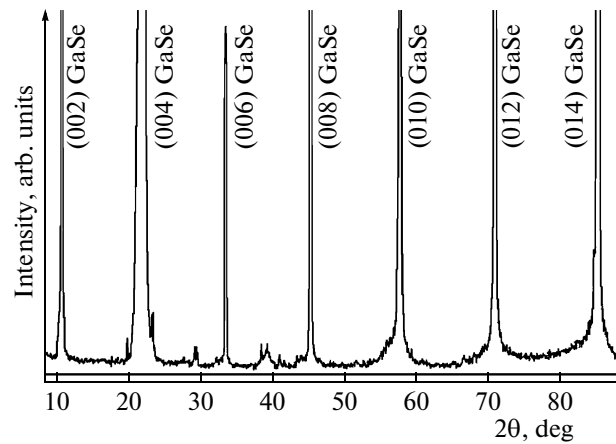


**Fig. 1.** X-ray diffraction pattern of the composite structure formed after  $\text{KNO}_3$  penetration into Van der Waals gaps of the GaSe layered crystal.

applied to In–Ga contacts arranged along the  $C$  axis of the GaSe(0001) crystal. The effect of the magnetic field on the carrier transport was studied at room temperature with structures placed between permanent magnet poles (the magnetic induction was  $B < 500 \text{ mT}$ ).

## 3. RESULTS AND DISCUSSION

In the X-ray diffraction pattern of layered GaSe crystals after  $\text{KNO}_3$  penetration into VdW gaps (Fig. 1), in addition to intense diffraction lines corresponding to reflections from (002), (004), (006), (008), (0010), (0012), and (0014) planes of the layered  $\epsilon$ -GaSe matrix, we can see low-intensity lines at angles  $2\Theta = (16.65^\circ \text{ and } 39.5^\circ)$ . They correspond to reflections from the (006) and (0014) planes, respectively, for 4H  $\delta$ -polytype GaSe modification with lattice parameters  $a = 3.7551$  and  $c = 31.9091 \text{ \AA}$ . This X-ray diffraction pattern also contains lines at angles  $2\Theta = 20.08^\circ, 23.50^\circ, 29.38^\circ, 29.68^\circ, 38.62^\circ$ , and  $41.17^\circ$  that correspond to a new unidentified phase. The result obtained suggests that the structure under study was formed due to chemical reactions between  $\text{KNO}_3$  and GaSe and in the presence of deformation interaction between crystalline inclusions (chemical reaction products) and the layered matrix. We note that this process, as well as the  $\text{KNO}_3$  FE introduction into GaSe [14, 15], was accompanied by pronounced thermal energy release. The study of the  $\text{KNO}_3$  introduction kinetics showed that this process is a “stage-by-stage” one [20] characteristic of ordered penetration of the material introduced into VdW gaps along the  $C$  axis of the layered crystal [21]. It is known that GaSe consists of layers incorporating Se–Ga–Ga–Se atomic planes. Depending on the number of such layers in the unit cell and on their relative orientation, the layered crystal can exist in various ( $\epsilon$ -,  $\gamma$ -,  $\beta$ -, and  $\delta$ -) polytype modifications [22]. Due to high anisotropy of GaSe elastic properties ( $C_{11}/C_{44} > 10$ ,  $C_{11}/C_{33} > 3$ ),

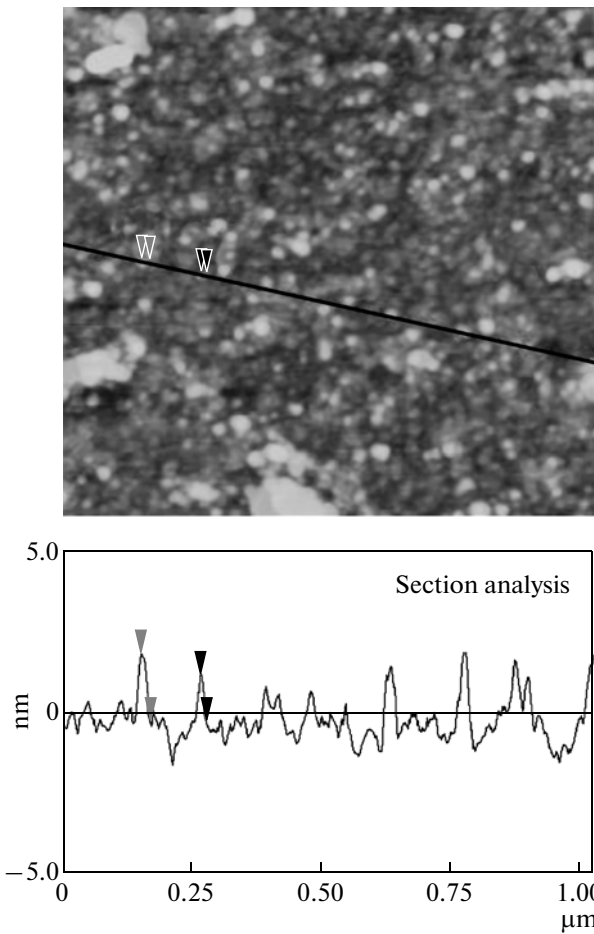


**Fig. 2.** Two-dimensional (2D) AFM image of the (0001) surface of GaSe layers after composite nanostructure formation. The distribution of height deviations of this surface along the line indicated in the 2D image is shown.

stress relaxation in this crystal is accompanied by displacement of layers with respect to each other [23]. Polytype modifications of layered crystals are described by various space groups. They can be formed by changing layer orientations with respect to each other during layered-crystal deformation. The lines corresponding to the GaSe  $\varepsilon$ -polytype were previously observed in X-ray diffraction patterns of Ni-GaSe barrier nanostructures [24] and nanoporous GaSe crystals [25], the formation of which was accompanied by  $\varepsilon$ -GaSe lattice deformation. A large number of NSs were observed in the image of the surface of the GaSe ( $\text{KNO}_3$ ) hybrid structure (Fig. 2); the image was obtained using a Nanoscope IIIa Dimension 3000SPM (Digital Instruments) atomic force microscope (AFM) in the Tapping mode in GaSe (0001) basal planes. The surface obtained by cleaving samples along layers at the structure synthesis temperature ( $T \approx 335^\circ\text{C}$ ) after introduction of  $\text{KNO}_3$  into the interlayer space was studied. The surface morphology was studied in air after cooling the samples to room temperature. Lateral sizes of an overwhelming majority of NSs

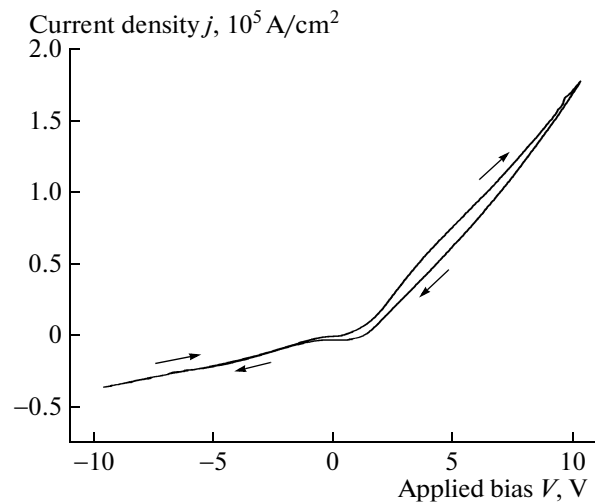


**Fig. 3.** Current–voltage characteristics of the composite nanostructure at  $T = 293$  K. Arrows indicate the direction of variation in the structure bias voltage.

do not exceed  $\sim 20$  nm, whereas vertical sizes (less than 2.5 nm) significantly exceed the interlayer spacing for GaSe ( $\sim 0.38$  nm) [22]. The distribution of the surface height deviation for the samples under study indicates the existence of depressions and protrusions (heights of  $\sim 1$ – $2$  nm, lateral sizes of  $\sim 120$ – $150$  nm) that contain NSs. Such a surface shape (complex corrugation) is typical of layered crystals with molecular (weak) bonds between layers in the presence of a large number of foreign material inclusions or nanoscale depressions on the surface. The surface is corrugated due to relaxation of stresses caused by the deformation interaction between defects and crystal layers [6–8, 24, 25].

The  $I$ – $V$  characteristics of composite structures are nonlinear (Fig. 3). Current hysteresis is observed in them. This effect was observed in  $I$ – $V$  characteristic of FE Schottky diodes [26] and was attributed to electric polarization switching in FE. Current flow mechanisms in these structures was studied by analyzing the impedance spectra  $Z'' = f(Z')$ , where  $Z'$  and  $Z''$  are, respectively, real and imaginary parts of the total complex impedance  $Z^* = Z' - jZ''$  of the structure. To this end, the frequency dependences of the impedance magnitude  $|Z| = (Z'^2 + Z''^2)^{1/2}$  and the phase angle  $\theta = f(\log f)$  (where  $\theta = \arctan(Z''/Z')$  and  $f$  is the frequency) were used. When analyzing the relaxation processes in the structures under conditions of high conductance, the frequency dependences of the phase angle [27] were used. A comparison of Nyquist diagrams for the composite structure and pure crystal (without introduced FE) shows that the  $\text{KNO}_3$  introduction into GaSe decreases the active conductance in a layered crystal (Fig. 4a, curves 1 and 2). The relaxation process is observed in the frequency dependence of the phase angle for the composite structure (indicated by arrows in the inset in Fig. 4b, curve 1), which is not observed in Bode diagrams for the pure layered

crystal (Fig. 4b, curve 2). It is shown by a curve that is asymmetric and a straight portion in the frequency range from  $f_1 = 2.52 \times 10^4$  to  $f_2 = 3.16 \times 10^4$  Hz. We note that relaxation processes in barrier structures based on layered crystals [24], processes associated with Maxwell–Wagner (interlayer) polarization [27], and processes involving impurity levels [28] manifest themselves in Bode diagrams as symmetric curves with broad peaks. The relaxation process observed for the pure layered crystal and composite structure in the higher frequency spectral region ( $f > 10^5$  Hz) (Fig. 4b) can be caused by carrier relaxation in GaSe near contacts [28]. The Nyquist diagram for the composite structure in the low-frequency spectral region ( $f < 10^5$  Hz) (Fig. 4a, curve 1) reflects two processes corresponding to different shapes of impedance diagrams. A relaxation process featuring an asymmetric shape (Fig. 4b, curve 1) is observed in the studied temperature range of 220–420 K for the structure under a dc bias voltage  $V_{dc}$  and at  $V_{dc} = 0$ . It almost does not shift along the frequency axis as temperature varies. The phase angle in this frequency region depends on the ac voltage amplitude  $V_{ac}$  of the measuring signal. This process can be associated with domain wall relaxation in nanoscale FE NSs arranged in the GaSe matrix. The domain nucleation time for FE materials is  $\sim 10^{-6}$ – $10^{-9}$  s [1], and the velocities of the domain walls responsible for polarization switching in FE capacitors are rather long [2]. It is known that bulk  $\text{KNO}_3$  crystals can exist in three phases ( $\alpha$ ,  $\beta$ ,  $\gamma$ ). At room temperature, the  $\alpha$ -phase is stable and features rhombic symmetry. Upon heating near  $T \approx 130^\circ\text{C}$ , the crystals exhibit transition from the  $\alpha$ -phase to the  $\beta$ -phase with rhombohedral symmetry. When crystals are cooled, the  $\beta$ – $\gamma$ -phase transition occurs near  $T \approx 124^\circ\text{C}$ , and the transition to the  $\alpha$ -phase occurs near  $T \approx 110^\circ\text{C}$ . Bulk crystals exhibit FE and semiconducting properties in the  $\gamma$ -phase [29]. The size and surface effects significantly affect the electrical properties of nanoscale systems [4, 10–12]. Anisotropic stresses arising during the deformation interaction between NSs and the matrix can cause the formation of the FE state in materials under conditions of constrained geometry (e.g., in  $\text{KTaO}_3$ , [4]). The presence of the gradient of elastic stresses or strains at the NS–matrix interface results in manifestation of the direct flexoelectric effect [4]. It consists in polarization (electric field) formation in the NS and can be observed during the formation of pyramidal nanoscale inclusions in the bulk of the anisotropic layered GaSe matrix. It is known that polarization switching processes in capacitor FE structures in a uniform electric field set in at individual local centers (polarization nucleation centers) and then propagate to macroscopic regions (about tens of  $\mu\text{m}$ ) [2]. As the electric field direction changes, the volume of already formed domains can be “compressed” and FE domains with opposite polarity can be nucleated [2]. It was experimentally shown that moving domain walls interact with FE

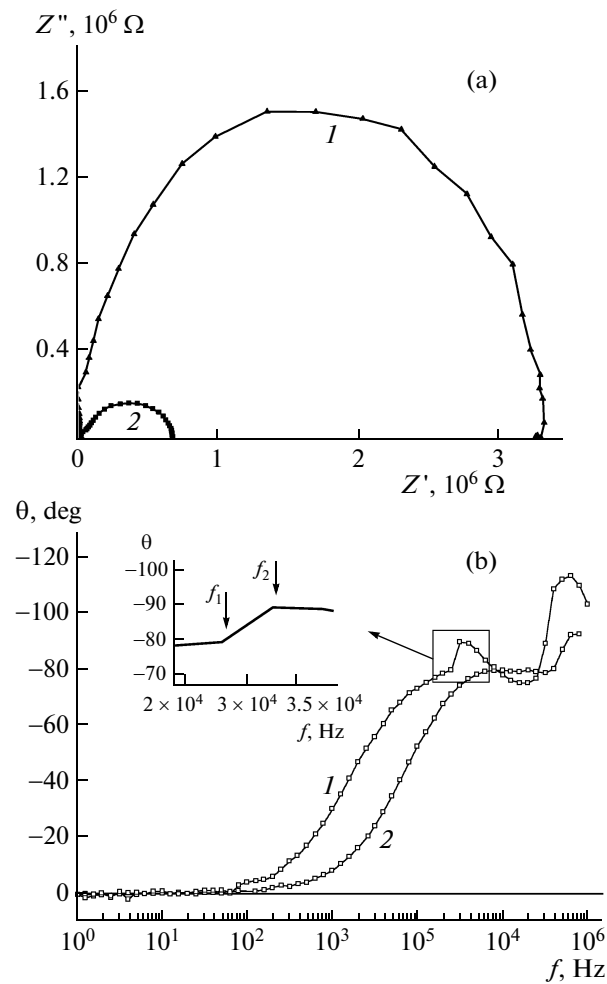


**Fig. 4.** Impedance spectra of the (1) composite nanostructure and (2)  $p$ -GaSe single crystal, measured at  $T = 293$  K at zero bias ( $V = 0$ ). (a) Nyquist diagrams  $Z'' = f(Z')$ ; (b) frequency dependences of the phase angle  $\theta$ . The inset shows the magnified asymmetric relaxation process associated with the deformation interaction between the layered matrix and ferroelectric nanoscale structures (NSs) formed as the ac voltage  $V_{ac}$  of the measuring signal is applied to the structure.

domain nuclei in the nanoscale material bulk [30]. Mobile domain walls in FE inclusions affect the properties of the surrounding LC matrix by means of long-range fields (electrostatic and elastic stress fields) [30]. Therefore, their dynamics, as an external ac voltage  $V_{ac}$  is applied to the structure, can be reflected in the frequency characteristics of the impedance of composite structures (Fig. 4b, curve 1).

The relaxation process, which exhibits a symmetric shape and is observed in the low-frequency region in the Nyquist diagrams (Fig. 4a) as a large semicircle, is associated with carrier flow in the layered GaSe matrix. It features the relaxation time  $\tau = RC$  and is simulated by a parallel ( $R \parallel C$ ) circuit, where  $C$  and  $R$  are the matrix capacitance and resistance. As the temperature increases (Fig. 5), semicircle centers shift

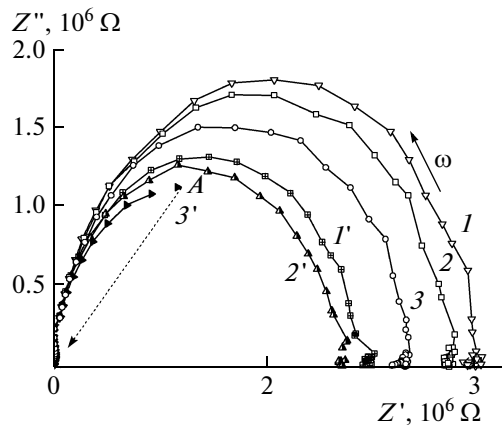


**Fig. 5.** Impedance spectra of the composite nanostructure, measured at zero bias  $V_{dc} = 0$  (1, 2, 3) and under bias  $V_{dc} = 7$  V (1', 2', 3') at temperatures  $T = (1, 1')$  240, (2, 2') 245, and (3, 3') 251 K. The polarity of the bias voltage applied to the structure corresponds to positive bias during  $I-V$  characteristic measurements (Fig. 3).

along the  $Z'$  axis to higher frequencies, and their diameters decrease, which is caused by an increase in the active conductance of the GaSe semiconductor matrix [24]. The temperature dependence of this conductance for the composite structure measured at  $V = 0$  exhibits an activation behavior. The activation energy  $E_{la} = 0.12$  eV was determined from the temperature dependence of the resistivity  $\rho \propto \exp(E_a/kT)$  of the composite nanostructure at zero bias. This value differs from  $E_a = 0.31$  eV for pure GaSe single crystals [24]. A decrease in the semicircle diameters (an increase in the GaSe matrix active conductance) at a dc bias voltage ( $V_{dc} > 6$  V is applied to the composite nanostructure) (Fig. 5, curves 1', 2', 3') is an unexpected observation. This effect manifests itself in the temperature region under study for composite structures and is not observed for pure layered crystals. At  $T = 251$  K and  $V_{dc} = 7$  V, the impedance spectrum is significantly transformed in the narrow frequency range  $\omega$  (in the vicinity of the point  $A$  in the Nyquist diagram), which is indicated by an arrow in Fig. 5 (curve 3'). As the temperature is lowered ( $T = 245$  K), such changes in the impedance spectrum are observed at the higher applied voltage  $V_{dc} \approx 8$  V. This effect is pronounced in the frequency dependences of the impedance magnitude of the composite nanostructure, measured at various values of  $V_{dc}$  at  $T = 300$  K (Fig. 6a). At the bias voltages  $V_{dc} = 6-9$  V, significant changes in the real (Fig. 6b) and imaginary (Fig. 6c) parts of the total complex impedance are observed in the low-frequency region of the impedance spectrum. In the low-frequency region of this spectrum, where the values of  $|Z|$  sharply decrease, the capacitance and active conductance of structures increase. The frequency range in which abrupt changes in the impedance are observed shift to higher frequencies in the

impedance spectrum as the bias voltage increases from  $V_{dc} = 6$  to 7 V. As the bias voltage varies within  $V_{dc} \approx 7-9$  V, the boundaries of this range ( $f_1 \approx 1580$  and  $f_2 \approx 1360$  Hz, indicated by arrows in Fig. 6a) remain unchanged. As the voltage further increases ( $V_{dc} > 9$  V), no abrupt changes in the frequency dependences of the impedance in the low-frequency region are observed. The impedance spectra measured at  $V_{dc} = 10$  and  $V_{dc} < 6$  V are almost identical (Fig. 6). When the bias voltage is changed in the reverse direction ( $V_{dc} < 10$  V), the low-frequency capacitance and active conductance of the structure reach their maximum values at  $V_{dc} \approx 6-8$  V. The dependence of the capacitance of the composite nanostructure on the dc bias voltage  $V_{dc}$ , measured at  $T = 300$  K at frequency  $f = 500$  Hz, is shown in Fig. 6d. We can see in Fig. 6c that the composite structure capacitance measured at  $V_{dc} = 7-9$  V monotonically increases in the low-frequency spectral range ( $10$  Hz  $< f < 3160$  Hz) with decreasing frequency (the values of  $Z''$  decrease). Such behavior of the capacitance is typical of the Maxwell–Wagner (M–W) effect, which takes place for heterogeneous ferroelectrically active structures [31]. It appears in thin-film  $\text{BiFeO}_3$  and Si MOS capacitors [32, 33], composite nanostructures based on the MCM-41 mesoporous dielectric matrix, and  $\text{NaNO}_2$  inclusions [12]. The M–W effect is associated with electric charge accumulation at the interface of various materials with different charge relaxation times. Charge accumulation at thin layer interfaces was observed for FE superlattices based on  $\text{Ba}_{1-x}\text{Sr}_x\text{TiO}_3$  in the case of an external voltage normally applied to layers [34]. The charge accumulation at the interface of two media, one of which has FE properties, depends on the electric polarization of the FE. This phenomenon is used in field-effect transistors with an FE gate [2]. A ferroelectric–semiconductor contact can induce a high “intrinsic” surface field, which results in pronounced band bending near the semiconductor surface and the appearance of a space charge accumulation/depletion region at the interface [35]. For a layered system consisting of components with different electrical parameters, the M–W theory predicts an increase in the active conductance with frequency. For heterogeneous ferroelectrically active unorderd composite structures, the frequency dependences of the real and imaginary parts of the complex permittivity and effective conductivity are monotonic [31]. The capacitance of capacitors based on  $\text{BiFeO}_3$  thin films [32] for which the M–W effect is observed at the interfaces between crystallites and depleted Schottky layers monotonically decreases with  $V$  and frequency in a wide frequency range of  $10^4-10^6$  Hz, which is caused by a change in the depletion region width near the interface. The nonmonotonic behavior of the frequency dependences of the impedance of  $\text{GaSe} < \text{KNO}_3$  composite nanostructures (Fig. 6) at certain applied voltages  $V_{dc}$  can be associated with electrical

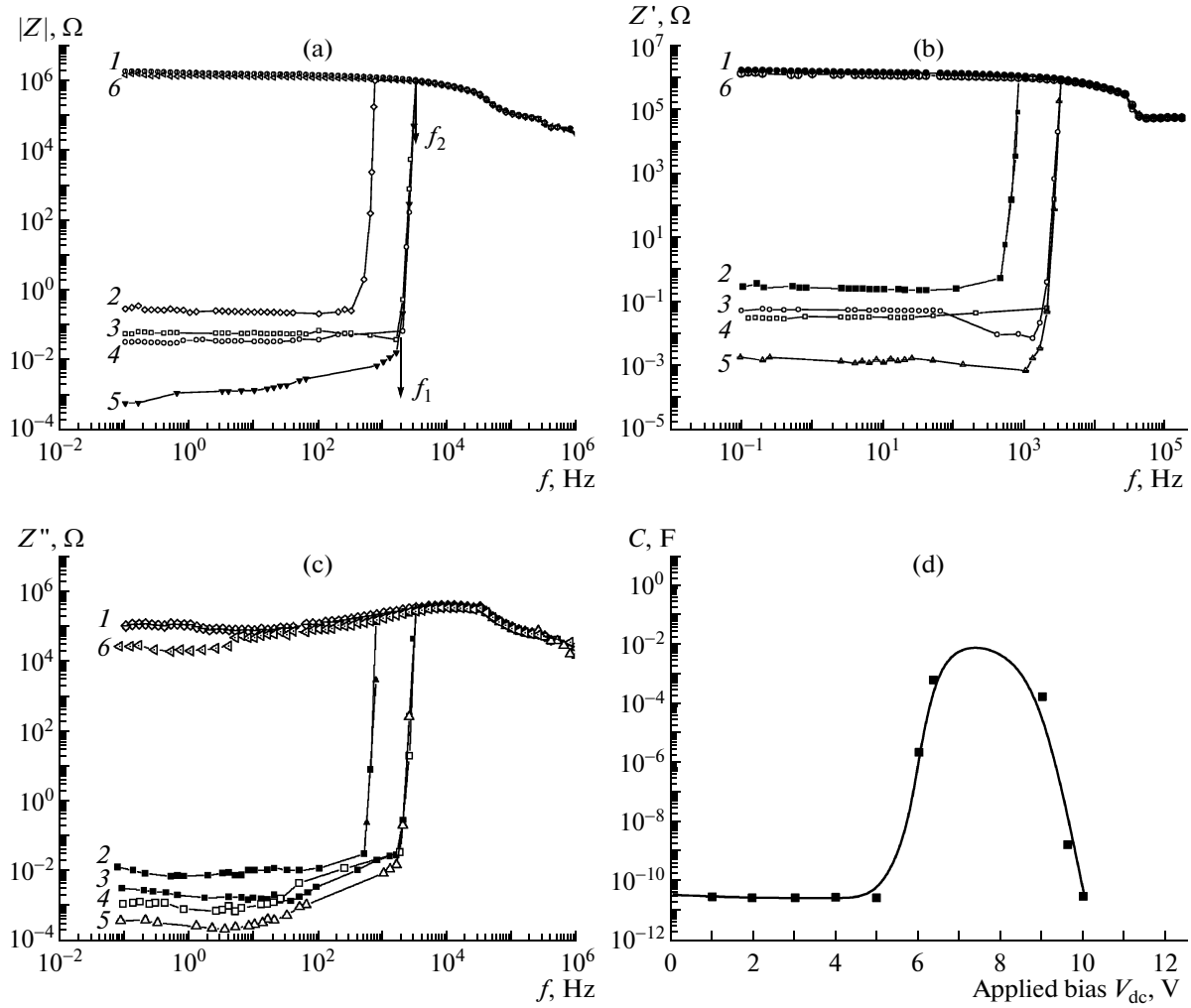


**Fig. 6.** (a, b, c) Frequency dependences of the composite nanostructure impedance, measured at  $T = 293$  K at bias voltages  $V_{dc}$  = (1) 0, (2) 6, (3) 7, (4) 8, (5) 9, and (6) 10 V. The polarity of the bias voltage applied to the structure corresponds to the positive bias in the  $I-V$  measurements (Fig. 3). (a) Frequency dependences of the impedance magnitude. Arrows indicate the boundaries of the frequency range in which abrupt changes in the impedance magnitude occur at  $V_{dc} = 7-9$  V, (b) frequency dependences of the real part  $Z'$  of the total impedance, (c) frequency dependences of the imaginary part  $Z''$  of the total impedance, and (d) the dependence of the composite nanostructure capacitance on the bias voltage  $V_{dc}$ .

polarization switching in FE NSs and with layered matrix restructurization in the NS localization region. In this case, due to the inverse piezoelectric effect in the FE NS, the deformation interaction between the NS and matrix results in structural changes in GaSe regions through which carrier transport occurs.

In the case of chemical reactions on the VdW surface, molecules and ions of the introduced material enter the layer structure from the liquid phase (melt) in defect regions (nanocavities) on this layered-crystal surface [7, 8]. Nanocavities are formed due to deformation processes in basal (0001) and pyramidal crystallographic planes of layered crystals [18] at high temperatures (above 573 K) after breaking chemical bonds between crystal atoms [6]. In the (0001) plane of the layer, the defect shape is hexagonal or triangular. Sur-

face defects with a hexagonal lateral cross section propagate to the crystal depth within a monolayer [6]. Nanocavities with triangular cross sections are shaped as an acute or truncated pyramids the apex of which is directed to the crystal depth (in parallel to the hexagonal symmetry axis of the layered crystal). Such defects propagate to a crystal depth of several lattice constants and encompass several crystal layers [6, 7, 25] (Fig. 7a). Nanoscale 3D inclusions formed after chemical reactions on the VdW surface fill these defects [7, 8]. Surface defects on the VdW surfaces of deformed crystals and layered-crystal epitaxial layers were observed in scanning tunneling microscopy (STM) images [36] and atomic-force microscopy (AFM) images [6, 7, 24, 25]. They can be orderly arranged on the VdW surface along crystallographic

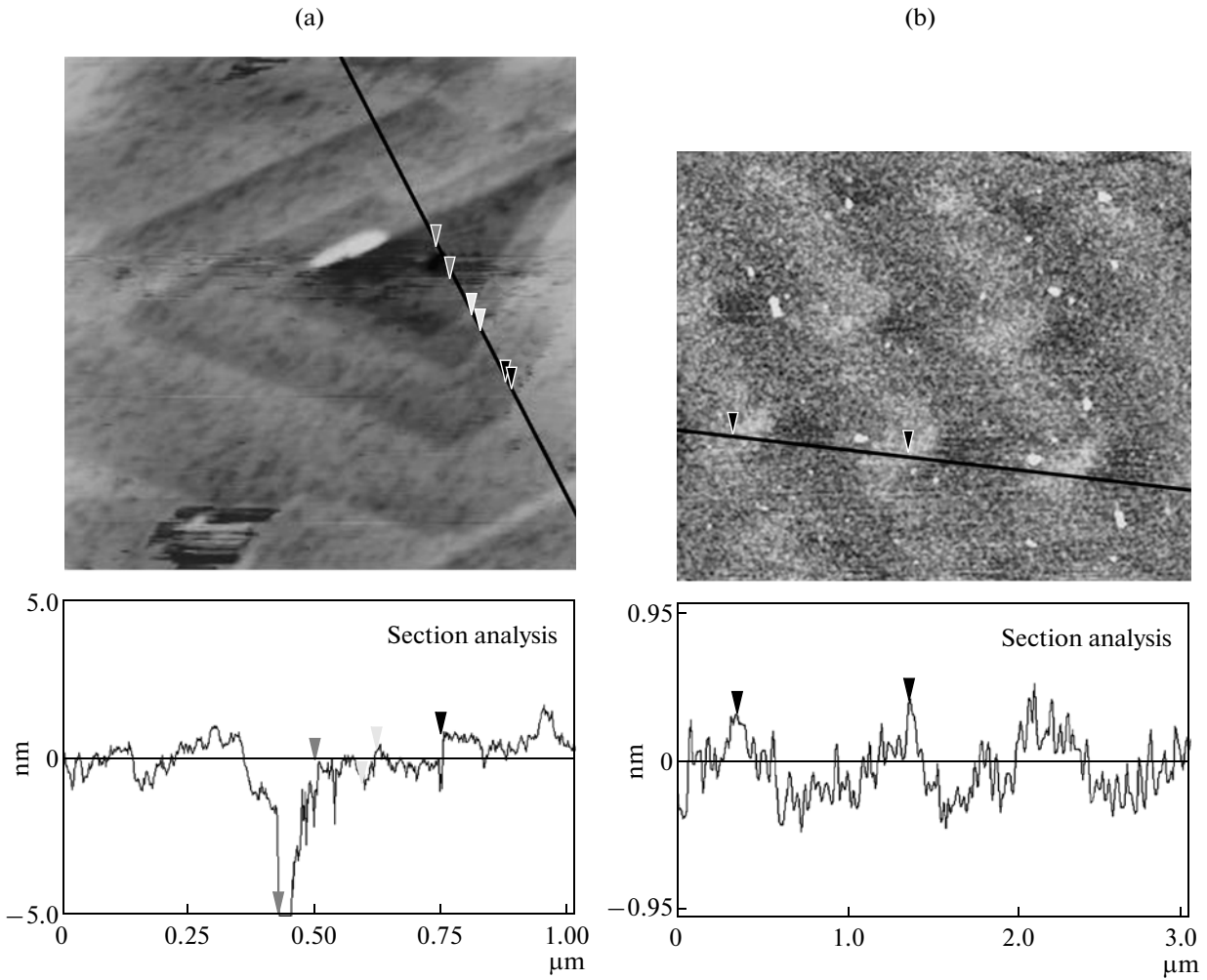


**Fig. 7.** AFM images of the (0001) defect surface of GaSe and InSe layered crystals [6, 7]. (a) 2D image of the nanocavity formed on the (0001) Van der Waals surface due to deformation processes along pyramidal crystallographic planes; (b) 2D image of the corrugated surface of the layered crystal, which contains nanoscale defects (nanocavities). The distribution of height deviations of this surface along the line indicated in the 2D image is shown.

directions of layered-crystal axes (Fig. 1b) or randomly arranged on this surface. After stress relaxation in layered-crystal layers containing nanoscale cavities or foreign impurities, a simple corrugated layered-crystal surface [7, 24] with periodic alternation of maxima (Fig. 7b) and (in the case of GaSe $\langle$ KNO<sub>3</sub> $\rangle$  nanostructures under study) a complex corrugated surface (Fig. 2) can be observed. Nanostructures with a corrugated surface fabricated based on ultrathin strained semiconductor films (InAs, InGaAs/GaAs, SiGe/Se) were considered as a system of quantum wells (QWs)[37].

Strains significantly affect the transverse (in the direction perpendicular to layer planes) conductance of layered crystals. The formation of nanocavities (Fig. 7a) and corrugated surfaces causes displacements of individual crystal layers with respect to each other [6–8, 25]. In this case, polytype phase transitions occur in layered crystals; these transitions are

accompanied by transformations of layered-crystal electron and phonon spectra with the formation of charge density waves (CDWs). CDWs in 2D layered dichalcogenides are associated with atomic displacements from the equilibrium position in the hexagonal lattice and changes in the electron density [22]. They were observed in layered graphite crystals intercalated with bromine [5] and in STM images of defect GaSe surfaces near the GaSe/Si(111) heterojunction [36]. Atomic displacements in individual crystal layers with respect to atoms of other layers caused significant periodic changes in the tunneling current flowing along the crystal C axis, which were observed in STM studies of the strained GaSe (0001) surface [38]. Anomalies in static and dynamic conductivity [19] and negative thermal expansion [39] of these layered crystals are associated with CDWs caused by Peierls polytype structural phase transitions occurring in InSe. Displacements of GaSe layers with respect to each other

during plastic deformation flow along pyramidal crystallographic planes during thermostimulated desorption of molecular hydrogen from nanoporous GaSe crystals resulted in significant changes in the transverse conductance in the low-frequency region of the impedance spectrum of these crystals [25].

During impedance studies of composite nanostructures, the voltage  $V = V_{dc} + V_{ac} \cos \omega t$  was applied to ohmic contacts arranged on GaSe (0001) planes ( $V_{dc}$  is the dc bias voltage,  $V_{ac}$  is the amplitude of the ac voltage of the measuring signal, and  $\omega = 2\pi f$  is the circular frequency of the measuring signal). The electric polarization in FE NSs varies with  $V$ . Periodic compression and expansion of NSs occurs due to the inverse piezoelectric effect. This effect is used in piezoresponse force microscopy (PFM) to study local polarization dynamics in FE nanocrystals, films, and capacitors [2]. Crystal layers can be considered as membranes (the Lifshitz membrane model [22]). A change in the deformation interaction between the NS and layers of the crystal matrix as the voltage  $V$  is applied can cause layer corrugation and changes in NS ferroelectric properties [4]. The composite structure under study can be presented as a semiconductor multiple quantum well (MQW) structure and as a superlattice with vertical transport during which sequential tunneling between adjacent QWs [40] occurs. The carrier transport typical of such structures was observed at room temperature in layered In<sub>2</sub>Se<sub>3</sub> crystals with narrow-gap nanoscale In<sub>6</sub>Se<sub>7</sub> inclusions [41]. QWs in the GaSe matrix can be formed by nanoscale FE inclusions (if they exhibit semiconducting properties) and due to crystal layer corrugation. The feature of the composite structure under consideration is that the geometrical shape of nanoscale layered crystal regions between adjacent NSs in the layered crystal (0001) basal plane can change due to the inverse piezoelectric effect in the FE NS as the voltage  $V$  is applied to the structure. In this case, the electric polarization of FE inclusions and the electric field localized in the QW arrangement region change.

An increase in the conductivity of GaSe<KNO<sub>3</sub>> composite structures at certain values of  $V_{dc}$  can be associated with carrier tunneling between QWs arranged along the  $C$  symmetry axis of the GaSe hexagonal crystal. A significant increase in the active conductance (decrease in semicircle diameters), which is observed in Fig. 5 at  $V_{dc} = 7$  V, is typical of the impedance spectra of tunneling barrier structures [24]. It is known that the total impedance of barrier semiconductor structures with a single QW depends on frequency [42]. The measured capacitance  $C_m$  of such a structure decreases with increasing frequency due to the series resistance  $R_s$  of the structure, which results in an increase in the conductance signal amplitude  $G_m$ . The frequency dependences of  $C_m$  and  $G_m$  of these structures are monotonic. The frequency dependences of the impedance of composite structures GaSe<KNO<sub>3</sub>> at  $V_{dc} \approx 6-9$  are nonmonotonic. Abrupt

changes in the conductance and capacitance of these structures, which are observed as the measuring signal frequency increases (Fig. 6), can be associated with the deformation interaction between the layered matrix and FE NS. A change in such interaction between components of composite nanostructures (e.g., due to the magnetostriction effect in Ni nanoparticles in BaTiO<sub>3</sub>-Ni nanostructures [43]) causes the same changes in the Nyquist diagram shape as are observed in Fig. 5 at  $V_{dc} > 6$  V. An abrupt change in the structure impedance spectrum at a certain frequency  $\omega$  (or in a narrow frequency range) (Fig. 5, curve 3') is typical of structural phase transitions during deformation of semiconductor crystals [44].

The mechanical properties of layered crystals with weak interlayer interactions (GaSe) during elastic deformation at the nanoscale level can be described by the model based on the crucial role of the interaction between atoms in the (0001) layer plane [45]. According to this model, the deformed VdW surface whose elastic properties are controlled by  $n$  interatomic interactions can be represented as  $n$  springs connected with each other (Fig. 8a). At small loads (less than 1 mN) applied along the crystal  $C$  axis, the dependence of the GaSe strain on the load is a sequence of sloped straight portions (corresponding to elastic deformation). They are separated by horizontal portions corresponding to plastic deformation [23]. Transition from one deformation type to another occurs almost instantaneously at certain loads ("pop-in events" [23]) and is accompanied by a shift (sliding) of layers with respect to each other. In the composite structures under study, GaSe layers that are fixed between FE NSs are bent as the voltage  $V_{dc}$  is applied to the structure (Fig. 8b). The bending  $\delta$  of these layers depends on the deformation interaction between the NS and layered-crystal matrix and their elastic constants. It depends on the normal component of the deforming force  $F$ , the distance between NSs, and the bending stiffness of layers. The bent thin GaSe layers exhibit forced oscillations as the external voltage  $V_{ac} \cos \omega t$  is applied to the composite structure.

It is conceivable that electric polarization switching occurs in the FE NS array as the voltage  $V$  increases. This effect for the structure under consideration occurs at  $V_{dc} \approx 6-7$  V. In this case, charges are accumulated at interfaces between FE NSs and GaSe and the bending of GaSe regions arranged between NSs increases. As the layered crystal is bent, individual layers are displaced with respect to each other (polytype phase transitions occur) with the formation of CDWs that affect the composite structure conductance. A structure can arise in the crystal formed by polytype and QW interlayers separated by tunneling barriers between which carriers can tunnel. The existence of  $\epsilon$ -GaSe crystalline inclusions of various polytypes ( $\gamma$ ,  $\beta$ ,  $\delta$ ) in the layered crystal is confirmed by photoluminescence measurements [46]. The formation of local regions with various polytype composi-

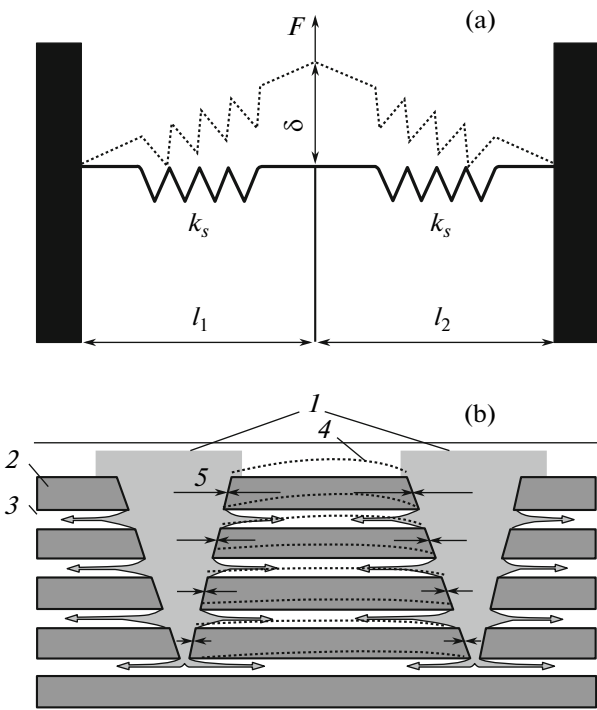


**Fig. 8.** (a) Schematic representation of an LC layer deformation [45]:  $F$  is the deforming force,  $\delta$  is the layer bending,  $l_1$  and  $l_2$  are the distances from the layer fixing point to the force  $F$  application point, and  $k_s$  is the spring stiffness coefficient. (b) Schematic representation of the region of the composite structures under study: (1) nanoscale ferroelectric structures (FE NSs), (2) GaSe layers in the absence of strong deformation interaction between inclusions and matrix ( $V_{dc} < 6$  V), (3) interlayer space in GaSe crystals, (4) bent GaSe layers under the bias voltage  $V_{dc} = 6\text{--}9$  V, and (5) forces of the deformation interaction between FE NSs and GaSe matrix.

tions and regions with residual stresses in these crystals was detected in the study of Raman spectra after irradiation and deformation of the crystals in the field of intense laser radiation [47].

The electric field distribution along the  $C$  axis and the charge redistribution between QWs affect the vertical transport in MQW structures [40] and optical and photoelectric properties of such structures. Previously, it was found that an external electric field directed in the plane of the GaSe layers significantly affects the intensity and spectral distribution of the photoluminescence of these crystals [46]. The observed features in the spectral distribution of the photoconductivity in structures  $\text{GaSe}\langle\text{NaNO}_2\rangle$  [14, 15] can be associated with the built-in electric field in these nanostructures in localization regions of FE nanoscale inclusions.

A significant decrease in the capacitance in  $\text{GaSe}\langle\text{KNO}_3\rangle$  structures as  $V_{dc}$  increases ( $V_{dc} > 9$  V (Fig. 6d) can be explained by the CDW mode suppression in the LC matrix under an electric field [19, 38].

At the same time, we note that the relaxation process that is observed in Bode diagrams (Fig. 4, curve 1) and is attributed to FE NS domain wall relaxation remains unchanged. This is indicative of an insignificant effect of the applied electric field on FE properties of NSs. The monotonic behavior of the impedance spectrum in the low-frequency region at  $V_{dc} = 10$  V (Figs. 6a–6c, curve 6) can also be caused by a layered-crystal structural change as  $V_{dc}$  increases as a result of the fast transition from the layered-crystal elastic deformation mode to the plastic deformation mode (“pop-in events” [23]). In this case, the shape of the corrugated surface of layered-crystal nanoscale regions arranged between NSs changes. It can be assumed that the structure is formed in this case, in which charge accumulation at interfaces between FE NSs and GaSe and carrier tunneling along the crystal  $C$  axis do not occur. The active transverse conductance and the low-frequency capacitance of such a composite structure sharply decrease.

The results of simulation of electric polarization switching in nanoscale FE objects show that there is a heavy dependence of the polarization switching voltage on the nanostructure morphology [17]. The effect of a significant increase in the low-frequency capacitance of  $\text{GaSe}\langle\text{KNO}_3\rangle$  composite nanostructures contained different in size NSs was observed at various dc bias voltages ( $V_{dc} < 10$  V). This can be associated with the dependence of electric polarization switching processes in these structures on the size, shape, and statistical characteristics of the NS ensemble.

When a composite structure to which an electrical bias  $V_{dc} = 6.5$  V was applied was placed into a weak magnetic field, the frequency range where significant changes in the impedance magnitude were observed (Fig. 9a) shifted to the high-frequency region. This effect was observed at  $T = 300$  K in a certain range of the magnetic field induction ( $B = 85\text{--}340$  mT). At  $B = 400$  mT, no abrupt changes in the impedance with frequency were observed (Fig. 9a, curve 4). In this case, the dependence of the impedance magnitude is monotonic, just as for composite nanostructures at  $V_{dc} = 0$  (Fig. 6a, curve 1). The magnetic field affects the relaxation process, which is associated with FE domain wall oscillation. This is seen from the comparison of the frequency dependences of the phase angle (Fig. 9b) for the structure under study, measured at  $B = 0$  (curve 1) and at  $B = 85$  and 340 mT (curves 2 and 3, respectively). At  $B = 400$  mT, this relaxation process is not observed in the frequency dependence of the phase angle of composite structures (Fig. 9, curve 4). The result obtained can be attributed to the magneto-plastic effect that takes place in FE crystals [16] and nonmagnetic crystals under the simultaneous action of electric and magnetic fields [48]. It is explained within the concept of spin-dependent electronic transitions in an external magnetic field, which results in a

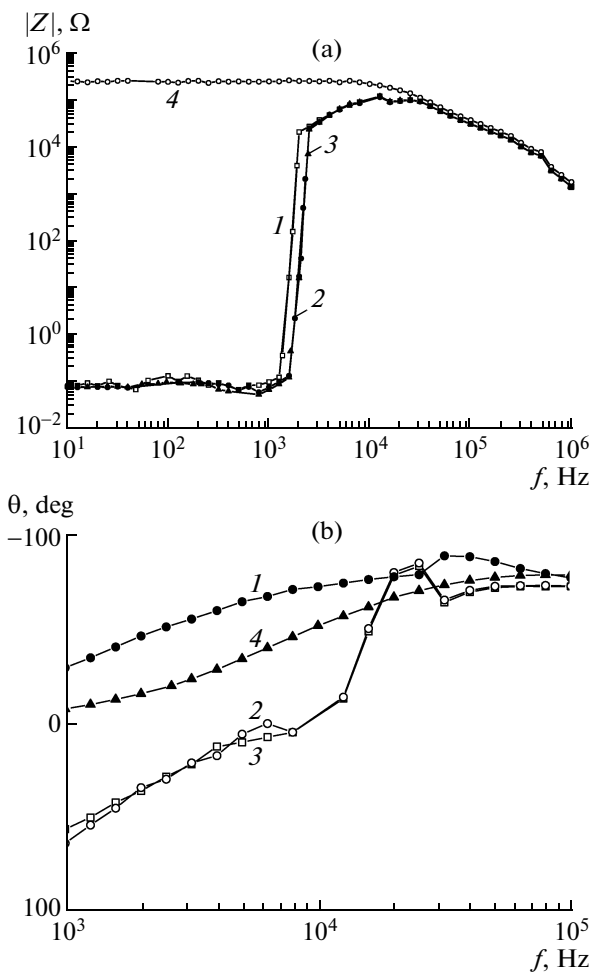


**Fig. 9.** Frequency dependences of the (a) impedance magnitude and (b) phase angle of the composite nanostructure, measured at  $T = 293$  K,  $V_{dc} = 6.5$  V, and magnetic inductions of the applied external magnetic field  $B = (1) 0$ , (2) 85, (3) 340, and (4) 400 mT. The polarity of the bias voltage applied to the structure corresponds to the positive bias in the  $I-V$  measurements (Fig. 3).

decrease in the interaction of impurity centers in FE crystals with dislocations. The magnetoplastic effect in these crystals manifests itself in a significant increase in the plastic deformation rate in a loaded sample as the magnetic field is turned on [16]. As a result, the yield stress and microhardness decrease and acoustic parameters (internal friction) of materials change. Application of a dc magnetic field to the composite nanostructure causes a change in the deformation interaction between the FE NS and layered-crystal matrix. In this case, the FE properties of nanoscale inclusions change [4] and the layered-crystal matrix structure changes in the NS localization region at the nanoscale level. This affects charge transport and accumulation processes in  $\text{GaSe}\langle\text{KNO}_3\rangle$  composite structures and manifests itself in the impedance spectra of these structures (Fig. 9).

#### 4. CONCLUSIONS

Progress in the development of nanostructures in which the semiconductor channel for carrier transport is combined with nanoscale ferroelectric layers (nanocrystals) is associated with the necessity of developing new technologies. They should provide high quality of the “semiconductor–ferroelectric” interface and the possibility of switching the electric polarization in nanoscale ferroelectric elements at low voltages (lower than 10 V) applied to structures. The high density of states that arise at layer interfaces during heterostructure formation by layer-by-layer growth of materials with highly mismatched lattices (of semiconductor and ferroelectric) results in spontaneous polarization screening in ferroelectric. The technology of ferroelectric material introduction into the interlayer space of layered semiconductor crystals with low density of surface states ( $\leq 10^{10}$  cm $^{-2}$ ) in layers with molecular bonds offers new opportunities for fabricating composite nanostructures with controlled ferroelectric properties. In this study, it is shown that such technology will make it possible to fabricate composite nanostructures consisting of a layered crystalline semiconductor GaSe matrix and 3D nanoscale crystalline ferroelectric inclusions orderly arranged along the  $C$  symmetry axis of this crystal. The carrier transport in these nanostructures depends on the polarity and value of the applied dc voltage. The carrier transport is associated with the electric polarization switching in the array of nanoscale ferroelectric inclusions and the formation of the electric field built in GaSe local regions. It is also controlled by the deformation interaction occurring between nanoscale inclusions and the layered crystal matrix. The carrier transport in these structures can also be controlled by applying an external voltage no higher than  $\sim 10$  V and a weak dc magnetic field ( $B < 400$  mT). A hysteresis was detected in the room-temperature  $I-V$  characteristics of the structures under study, which is related to electric polarization switching in nanoscale inclusion. This offers the possibility of using these structures as memory devices in information technologies. After switching the electric polarization, a significant increase in the capacitance of composite nanostructures is observed in the low-frequency region of the impedance spectrum, which is attributed to the Maxwell–Wagner effect. This phenomenon can be used for developing efficient electrical-energy storage devices and filter capacitors based on these nanostructures. It was found that the voltage of electric polarization switching depends on the nanostructure morphology. The dependence of the impedance spectra of composite structures on the voltage and magnetic field is associated with quantum-confinement effects during current flow through the structure under conditions of changing the deformation interaction, which takes place between the layered matrix and nanoscale ferroelectric inclusions under electric and magnetic fields. This interaction can change due to the inverse piezo-

electric effect and the magnetoplastic effect in inclusions. In this case, polytype structural Peierls phase transitions can occur in the GaSe layered matrix and the geometrical shape of the layer surface can change in nanoscale layered-crystal regions through which the vertical transport of carriers occurs.

## REFERENCES

1. V. M. Fridkin, R. V. Gainutdinov, and S. Dyusharm, Usp. Fiz. Nauk **180**, 209 (2010) [Phys. Usp. **53**, 199 (2010)].
2. S. V. Kalinin, A. N. Morozovska, L. Q. Chen, and B. J. Rodriguez, Rep. Progr. Phys. **73**, 056502 (2010).
3. B. J. Rodriguez, S. Jesse, M. Alexe, and S. V. Kalinin, Adv. Matter. **20**, 109 (2008).
4. M. D. Glinchuk, E. A. Eliseev, and A. N. Morozovska, Ukr. J. Phys. Rev. **5**, 34 (2009).
5. F. Batallan, I. Rosenman, Ch. Simon, and G. Furdin, Mater. Rec. Soc. Symp. Proc. **20**, 129 (1983).
6. A. P. Bakhtinov, V. N. Vodop'yanov, E. I. Slyn'ko, Z. D. Kovalyuk, and O. S. Litvin, Pis'ma Zh. Tekh. Fiz. **33** (2), 80 (2007) [Tech. Phys. Lett. **33**, 86 (2007)].
7. S. I. Drapak, A. P. Bakhtinov, S. V. Gavrylyuk, Z. D. Kovalyuk, and O. S. Lytvyn, Superlat. Microstruct. **44**, 563 (2008).
8. S. I. Drapak, S. V. Gavrylyuk, V. M. Kaminskii, and Z. D. Kovalyuk, Zh. Tekh. Fiz. **78**, 112 (2008) [Tech. Phys. **53**, 1215 (2008)].
9. A. I. Dmitriev, Z. D. Kovalyuk, G. V. Lashkarev, V. I. Lazorenko, M. Yu. Gusev, A. N. Zyuganov, and P. S. Smertenko, Solid State Commun. **75**, 465 (1990).
10. S. V. Baryshnikov, E. V. Stukova, E. V. Charnaya, Cheng Tien, M. K. Lee, W. Bohlmann, and D. Michel, Fiz. Tverd. Tela **48**, 551 (2006) [Phys. Solid State **48**, 593 (2006)].
11. S. V. Baryshnikov, E. V. Charnaya, A. Yu. Milinskii, E. V. Stukova, Cheng Tien, W. Bohlmann, and D. Michel, Fiz. Tverd. Tela **51**, 1172 (2009) [Phys. Solid State **51**, 1243 (2009)].
12. S. V. Baryshnikov, E. V. Charnaya, Cheng Tien, M. K. Lee, D. Michel, N. P. Andriyanova, and E. V. Stukova, Fiz. Tverd. Tela **49**, 751 (2007) [Phys. Solid State **49**, 791 (2007)].
13. V. V. Netyaga, I. I. Grigorchak, and Z. D. Kovalyuk, Fiz. Tverd. Tela **34**, 3608 (1992) [Sov. Phys. Solid State **34**, 1933 (1992)].
14. V. V. Netyaga, I. I. Grigorchak, and Z. D. Kovalyuk, Fiz. Tekh. Poluprovodn. **27**, 1220 (1993) [Semiconductors **27**, 673 (1993)].
15. I. I. Grigorchak, V. V. Netyaga, and Z. D. Kovalyuk, J. Phys.: Condens. Matter **9**, L191 (1997).
16. B. I. Smirnov, N. N. Peschanskaya, and V. I. Nikolaev, Fiz. Tverd. Tela **43**, 2154 (2001) [Phys. Solid State **43**, 2250 (2001)].
17. R. Ahluwalia, Nathaniel Ng, and D. J. Srolovitz, Nanotechnolohy **20**, 445709 (2009).
18. G. L. Belen'kii, V. A. Goncharov, V. D. Negrii, Yu. A. Osip'yan, and R. A. Suleimanov, Fiz. Tverd. Tela **26**, 3144 (1984) [Sov. Phys. Solid State **26**, 1893 (1984)].
19. G. V. Lashkarev, A. I. Dmitriev, A. A. Baida, Z. D. Kovalyuk, M. V. Kondrin, and A. A. Pronin, Fiz. Tekh. Poluprovodn. **37**, 145 (2003) [Semiconductors **37**, 134 (2003)].
20. I. I. Grigorchak, V. V. Netyaga, I. D. Koz'mik, K. D. Tovstyuk, Z. D. Kovalyuk, B. P. Bakhmatyuk, and S. Ya. Golub', Pis'ma Zh. Tekh. Fiz. **15** (4), 87 (1989) [Tech. Phys. Lett. **89**, 158 (2009)].
21. D. Kaluarachchi and R. F. Frindt, Phys. Rev. B **28**, 3663 (1983).
22. G. L. Belen'kii, E. Yu. Salaev, and R. A. Suleimanov, Usp. Fiz. Nauk **155**, 89 (1988) [Sov. Phys. Usp. **31**, 434 (1988)].
23. D. H. Mosca, N. Mattoso, C. M. Lepienski, W. Veiga, I. Mazzaro, V. H. Etgens, and M. Eddrief, J. Appl. Phys. **91**, 140 (2002).
24. A. P. Bakhtinov, V. N. Vodop'yanov, Z. D. Kovalyuk, V. V. Netyaga, and O. S. Litvin, Fiz. Tekh. Poluprovodn. **44**, 180 (2010) [Semiconductors **44**, 171 (2010)].
25. Z. D. Kovalyuk, A. P. Bakhtinov, V. N. Vodop'yanov, A. V. Zaslonskin, and V. V. Netyaga, in *Carbon Nanomaterials in Clean Energy Hydrogen Systems*, Ed. by B. Baranowski, S. Yu. Zaginaichenko, D. V. Schur, V. V. Skorokhod, and A. Veziroglu (Springer, Netherlands, 2009).
26. P. w. M. Blom, R. M. Wolf, J. F. M. Cillessen, and M. P. C. Krijn, Phys. Rev. Lett. **73**, 2107 (1994).
27. A. S. Bogatin, I. V. Lisitsa, and S. A. Bogatina, Pis'ma Zh. Tekh. Fiz. **28** (18), 61 (2002) [Tech. Phys. Lett. **28**, 779 (2002)].
28. Y. Y. Proskuryakov, K. Durose, B. M. Taele, and S. Oelting, J. Appl. Phys. **102**, 024504 (2007).
29. B. Erdinc and H. Akkus, Phys. Scripta **79**, 025601 (2009).
30. V. R. Aravind, A. N. Morozovska, I. Grinberg, S. Bhattacharyya, Y. Li, S. Jesse, S. Choudhury, P. Wu, K. Seal, E. A. Eliseev, S. V. Svechnikov, D. Lee, S. R. Phillpot, L. Q. Chen, A. M. Rappe, V. Gopalan, and S. V. Kalinin, arXiv:**1004**, 0797.
31. A. V. Turik, G. S. Radchenko, A. I. Chernobabov, S. A. Turik, and V. V. Suprunov, Fiz. Tverd. Tela **48**, 1088 (2006) [Phys. Solid State **48**, 1157 (2006)].
32. G. Z. Liu, C. Wang, C.-C. Wang, J. Qiu, M. He, J. Xing, K.-Jin, H.-B. Lu, and G.-Z. Yang, Appl. Phys. Lett. **92**, 122903 (2008).
33. K. B. Jinesh, Y. Lamy, J. H. Klootwijk, and W. F. A. Besling, Appl. Phys. Lett. **95**, 122903 (2009).
34. D. O'Neill, R. M. Bowman, and J. M. Gregg, Appl. Phys. Lett. **77**, 1520 (2000).
35. V. M. Fridkin, *Ferroelectric Semiconductors* (Nauka, Moscow, 1976).
36. T. Ohta, A. Klust, J. A. Adams, Q. Yu, M. A. Olmstead, and F. S. Ohuchi, Phys. Rev. B **69**, 125322 (2004).

37. A. B. Vorob'ev, V. Ya. Prinz, Yu. S. Yukecheva, and A. I. Toropov, *Physica E* **23**, 171 (2004).
38. A. Humberta, F. Salvana, and C. Moutteta, *Surf. Sci.* **181**, 307 (1987).
39. A. I. Dmitriev, V. M. Kaminskii, G. V. Lashkarev, P. E. Butorin, Z. D. Kovalyuk, V. I. Ivanov, and A. I. Beskrovnyi, *Fiz. Tverd. Tela* **51**, 2207 (2009) [*Phys. Solid State* **51**, 2342 (2009)].
40. O. V. Pupysheva, A. V. Dmitriev, A. A. Farajian, H. Mizuseki, and Y. Kawazoe, *J. Appl. Phys.* **100**, 033718 (2006).
41. S. I. Drapak, S. V. Gavrilyuk, and Z. D. Kovalyuk, *Pis'ma Zh. Tekh. Fiz.* **35** (12), 66 (2009) [*Tech. Phys. Lett.* **35**, 569 (2009)].
42. P. N. Broukov, T. Benyattou, G. Guillot, and S. A. Clarc, *J. Appl. Phys.* **77**, 240 (1995).
43. L. Qiao and X. Bi, *Appl. Phys. Lett.* **92**, 214101 (2008).
44. C. He, C. Gao, Y. Ma, M. Li, A. Hao, X. Huang, B. Liu, D. Zhang, C. Yu, G. Zou, Y. Li, H. Li, X. Li, and J. Liu, *Appl. Phys. Lett.* **91**, 092124 (2007).
45. J. Fraxedas, S. Garcia-Manyes, P. Gorostiza, and F. Sanz, *Proc. Natl. Acad. Sci. USA* **99**, 5228 (2002).
46. Y. Fan, M. Bauer, L. Kador, K. R. Allakhverdiev, and E. Yu. Salaev, *J. Appl. Phys.* **91**, 1081 (2002).
47. A. Baidullaeva, Z. K. Vlasenko, B. K. Dauletmuratov, L. F. Kuzan, and P. E. Mozol', *Fiz. Tekh. Poluprovodn.* **39**, 405 (2005) [*Semiconductors* **39**, 381 (2005)].
48. A. A. Urusovskaya, V. I. Al'shits, N. N. Bekkauer, and A. E. Smirnov, *Fiz. Tverd. Tela* **42**, 267 (2000) [*Phys. Solid State* **42**, 274 (2000)].

*Translated by A. Kazantsev*